A sensor kinase controls turgor-driven plant infection by the rice blast fungus

Article (Accepted Version)

A sensor kinase controls turgor-driven plant infection by the rice blast fungus

Lauren S. Ryder[1, 4], Yasin F. Dagdas[1, 4], Michael J. Kershaw[1], Chandrasekhar Venkataraman[3], Anotida Madzvamuse[3], Xia Yan[1, 4], Neftaly Cruz-Mireles[4], Darren M. Soanes[1], Miriam Oses-Ruiz[1, 4], Vanessa Styles[3], Jan Sklenar[4], Frank L.H. Menke[4], Nicholas J. Talbot[1, 4]*

[1] Department of Biosciences, The University of Exeter, Geoffrey Pope Building, Stocker Road, Exeter EX4 4QD, UK
[2] School of Mathematics and Statistics, Mathematical Institute, University of St. Andrews, North Haugh, St Andrews KY16 9SS, UK
[3] School of Mathematical and Physical Sciences, Department of Mathematics, University of Sussex, Brighton, BN1 9QH. UK
[4] The Sainsbury Laboratory, University of East Anglia, Colney Lane, NR4 7UH, Norwich, UK
*To whom correspondence should be addressed (nick.talbot@tsl.ac.uk)

The blast fungus *Magnaporthe oryzae* gains entry to its host plant by means of a specialized pressure-generating infection cell called an appressorium, which physically ruptures the leaf cuticle[1,2]. Turgor is applied as an enormous invasive force by septin-mediated reorganization of the cytoskeleton and actin-dependent protrusion of a rigid penetration hypha[3]. However, the molecular mechanisms that regulate the generation of turgor pressure during appressorium- mediated infection of plants remain poorly understood. Here we show that a turgor-sensing histidine–aspartate kinase, Sln1, enables the appressorium to sense when a critical turgor threshold has been reached and thereby facilitates host penetration. We found that the Sln1 sensor localizes to the appressorium pore in a pressure- dependent manner, which is consistent with the predictions of a mathematical model for plant infection. A Δ*sln1* mutant generates excess intracellular appressorium turgor, produces hyper-melanized non-functional appressoria and does not organize the septins and polarity determinants that are required for leaf infection. Sln1 acts in parallel with the protein kinase C cell-integrity pathway as a regulator of cAMP-dependent signalling by protein kinase A. Pkc1 phosphorylates the NADPH oxidase regulator NoxR and, collectively, these signalling pathways modulate appressorium turgor and trigger the generation of invasive force to cause blast disease.

Plant pathogenic fungi cause many of the world's most devastating crop diseases, and pose a constant threat to global food security[4,5]. The fungus *Magnaporthe oryzae* causes rice blast the most widespread and serious disease of rice[1] as well as wheat blast, which recently spread from South America to Bangladesh, threatening wheat production across South Asia[6,7].

To infect plants, *M. oryzae* develops a specialized infection cell called an appressorium[2] that ruptures the leaf cuticle using huge invasive force. The appressorium generates turgor of up to 8.0 MPa by accumulating high concentrations of glycerol and other polyols[8]. A differentiated cell wall that is rich in melanin is essential for the generation of turgor, acting as a rigid structural barrier to prevent the

efflux of solutes[8,9]. The translation of appressorium turgor into mechanical force causes a narrow penetration hypha to emerge from the base of the appressorium and breach the cuticle of the rice leaf[1]. Septin GTPases form a toroidal, hetero-oligomeric complex at the appressorium pore, and this complex scaffolds cortical F-actin at the point of plant infection. Septins provide cortical rigidity and act as a diffusion barrier for polarity determinants that mediate membrane curvature and protrusion of the penetration hypha[3]. Septin-mediated reorientation of F-actin also requires the regulated synthesis of reactive oxygen species by NADPH oxidases (NOX)[10].

We set out to investigate how the internal pressure of the appressorium is modulated to control repolarization. We reasoned that the appressorium must reach a critical turgor threshold to trigger septin-mediated reorganization of the cytoskeleton. To test this idea, we first artificially lowered the turgor of the appressorium, and quantified the frequency of assembly of septin rings and the resulting disease lesions (Fig. 1). We observed fewer lesions when high concentrations of glycerol were applied to rice seedlings, demonstrating a relationship between appressorium turgor and infection (Fig. 1a, b). By contrast, application of glycerol to intact rice leaves had no effect (Extended Data Fig. 1). Septin organization was also impaired after treatment of appressoria with glycerol, and by treatment with the melanin biosynthesis inhibitor tricyclazole when applied before 16 hours post-inoculation (h.p.i.) (Fig. 1c, Extended Data Fig. 2a). Furthermore, septins and F-actin were mislocalized in the melanin deficient mutants Δ*alb1*, Δ*rsy1* and Δ*buf1*, which fail to generate sufficient turgor for plant infection[9,11] (Fig. 1d, Extended Data Fig. 2b). We conclude that septin organization at the appressorium pore requires a critical threshold of cellular turgor and that this is essential for plant infection.

We postulated that a turgor sensor in appressoria must be necessary for the modulation of turgor pressure. To test this idea, we developed a mathematical model that couples geometric evolution laws for motion of the fungus and leaf surface with equations for the biosynthesis of melanin at the appressorium cortex, recruitment of septins and reorganization of F-actin (see Supplementary Information for a description and critical analysis of both the utility and the limitations of the mathematical model). A simulation of the model shows dynamics of appressorium repolarization that are consistent with experimental observations, and predicts that a mutant that lacks the turgor sensor will develop non-functional, hyper-melanized appressoria with excess turgor and aberrant deposition of septin and actin (Extended Data Fig. 3a, b; Supplementary Videos 1 and 2).

We next set out to identify the potential turgor sensor in *M. oryzae*. We noted that among potential candidates, *M. oryzae* possesses a homologue of the Sln1 histidine aspartate sensor kinase a known yeast osmosensor that modulates hyperosmotic adaptation through the high osmolarity glycerol (HOG) MAPK pathway[12]. The *HOG1* homologue in *M. oryzae*, *OSM1*, is dispensable for pathogenicity and glycerol production, suggesting that regulation of turgor is *OSM1*-independent[13]. *SLN1* was previously shown to be necessary for virulence in *M. oryzae*, but its function is unknown[14] (Fig. 2a, b, Extended Data Fig. 3c). Appressoria of a Δ*sln1* mutant generate extremely high turgor, as measured by incipient cytorrhysis[14] (Fig. 2c), but are non-functional. Live-cell imaging of *M. oryzae* that express a functional Sln1–GFP fusion showed that Sln1 localizes to the appressorium pore as infection cells generate pressure (Extended Data Fig. 3d, Supplementary Video 3). Localization of Sln1 was

also sensitive to changes in turgor, and exposure to hyper- osmotic glycerol led to Sln1 mislocalization (Fig. 2d) whereas the nuclear marker histone H1–GFP was unaffected (Extended Data Fig. 3e). The Δ*sln1* mutant also formed hyper-melanized appressoria (Fig. 2e) a phenotype that was partially reversed by exposure to tricyclazole (Fig. 2e). Applying hyperosmotic stress to appressoria also enhanced the deposition of melanin in the wild-type Guy11 strain of *M. oryzae* (Extended Data Fig. 4), suggesting that Sln1 modulates melanization of the appressorium once sufficient turgor has been generated.

To identify cellular functions that are controlled by Sln1, we used RNA sequencing (RNA-seq) to compare global changes in gene expression in a Δ*sln1* mutant to wild-type Guy11 during appressorium development. Among 1,982 genes that were affected in expression by loss of *SLN1* at 16 h.p.i., the melanin biosynthetic genes *RSY1* and *BUF1* were significantly upregulated in the Δ*sln1* mutant consistent with increased melanization (Fig. 2e, Extended Data Fig. 5a). Furthermore, Sln1–GFP was mislocalized in Δ*alb1*, Δ*rsy1* and Δ*buf1* mutants (Fig. 2f). Notably, the *M. oryzae* response regulator mutants Δ*ssk1* and Δ*skn7* also display enhanced melanization[15] and in *Cryptococcus neoformans*, Δ*skn7*, Δ*ssk1* and Δ*tco1* mutants show similar phenotypes[16]. We reasoned that Sln1 negatively regulates melanin biosynthesis and turgor generation, and triggers repolarization of the appressorium. We therefore tested whether the organization of the septin ring and toroidal F-actin network in appressoria was affected in Δ*sln1* mutants Sep5–GFP and LifeAct–RFP (a marker of F-actin) were both mislocalized in Δ*sln1* mutants (Fig. 2g, Extended Data Fig. 5b). Septin organization was also impaired in Δ*alb1* mutants (Extended Data Fig. 5c), and disrupted in Δ*buf1* mutants, which are blocked at a later stage in production of 1, 8-dihydroxynaphthalene (DHN)-melanin (Fig. 1d). The Δ*sln1* mutant therefore continues to generate turgor in the appressorium, but reorganization of septins and formation of the penetration peg do not occur.

To investigate the putative Sln1 turgor-sensing complex, we immuno- precipitated Sln1–GFP from appressorium protein extracts at 16 h.p.i. and performed liquid chromatography tandem mass spectrometry (LC–MS/MS) (Fig. 3a). Sln1 putatively interacts with two mechano- sensitive ion-channel proteins, Mic1 and Mic3, similarly to previously described yeast proteins that respond to osmotic shock[17]. Blocking mechanosensitive ion channels with gadolinium and verapamil prevented appressorium formation (Extended Data Fig. 6), and although Mic1, Mic2 and Mic3 were individually dispensable for virulence, Mic2–GFP localized to the centre of the appressorium pore in an *SLN1*- dependent manner (Extended Data Fig. 7a–c). Sln1 also putatively interacts with two chitin synthases that are required for biosynthesis of the fungal cell wall, Chs4 and Chs5, and staining Δ*sln1* with calcofluor white revealed aberrant deposition of chitin within the cell wall of the appressorium (Extended Data Fig. 8a). This mirrors a previous study in *Arabidopsis thaliana*, which showed that *TOD1*—an alkaline ceramidase that regulates the turgor of guard cells and pollen tubes—acts by regulating cell-wall remodelling[18]. In addition, Sln1 interacts with Sum1, the regulatory subunit of cAMP-dependent protein kinase A (PKA), in both co-immunoprecipitation and yeast two-hybrid analyses (Fig. 3a, Extended Data Fig. 8b). PKA regulates the mobilization of lipid bodies and lipolysis, which leads to glycerol-dependent generation of turgor in *M. oryzae*[19]. The expression of *SUM1* is increased in a Δ*sln1* mutant, suggesting that Sln1 negatively regulates the PKA pathway to modulate the biosynthesis of glycerol (Fig. 3b). Consistent with this idea, the PKA drug

inhibitor H-89 disrupts the organization of the appressorium pore in a dose-dependent manner, and localization of Sep5–GFP, gelsolin–GFP and Sln1–GFP is also impaired in a Δ*cpka* mutant (GenBank accession Q01143; Fig. 3c, Extended Data Fig. 9a–c). CpkA–GFP localizes to the appressorium pore (Fig. 3d) during the onset of turgor, consistent with its increased gene expression at this time (Fig. 3e).

Sln1 can also interact with protein kinase C (Pkc1), the central regulator of the cell-integrity pathway (Fig. 3b, Extended Data Fig. 8b). *PKC1* is an essential gene in *M. oryzae*, so to test its function in appressorium repolarization we used an allelic replacement mutant, *PKC1*^{AS}, which expresses an analogue-sensitive (Shokat) version of the kinase that is specifically sensitive to the ATP analogue 1NA- PP1[20]. Inhibition of Pkc1 by 1NA-PP1 disrupted the organization of Sep3–GFP, LifeAct–RFP and gelsolin–GFP at the appressorium pore (Fig. 3f), which was reversed by removal of 1Na-PP1 (Extended Data Fig. 10a). RNA-seq analysis of the *PKC1*^{AS} mutant in the presence or absence of 1NA-PP1 also showed a significant reduction in the expression of *NOX1, NOX2* and *NOXR* after 24 h[20] (Extended Data Fig. 10b). Furthermore, yeast two-hybrid analysis revealed transient interactions between Nox1, Nox2, NoxR and Pkc1 (Extended Data Fig. 10c). This is consistent with studies in humans that have demonstrated that PKC is required for phosphorylation of gp91phox (Nox2), and that this phosphorylation enhances the diaphorase activity of gp91phox and its binding to Rac2, p67phox (NoxR) and p47phox (Bem1)[21]. By phosphoproteomic analysis, we observed that Pkc1 phosphorylates NoxR at serine 321 (Extended Data Fig. 10d, Supplementary Table 2), consistent with activation of the NADPH oxidase complex[10,22] (which is necessary for septin-dependent plant infection) by Pkc1. Notably, Pkc1 also phosphorylates the phosphodiesterase PdeH which regulates the PKA pathway at serine 883, in addition to phosphorylating other proteins that are predicted to be involved in the sensing of turgor (Supplementary Table 2). Incipient cytorrhysis of a Δ*pdeH* mutant shows that it generates excess appressorium turgor, suggesting that PdeH is regulated by Sln1 (Extended Data Fig. 10e). PdeH in *M. oryzae* was previously shown to mediate cross-talk between the PKA, HOG and cell-integrity pathways[23] consistent with a role in turgor sensing.

Finally, a cell-cycle checkpoint, triggered by the generation of appressorium turgor and by melanization, is known to regulate septin dependent infection[24]. We therefore blocked the progression of cells into S phase by treatment with hydroxyurea, which prevented Sln1 recruitment to the appressorium pore (Extended Data Fig. 10f). Operation of this cell-cycle checkpoint is thus critical to the sensing of turgor in appressoria.

When considered together with our mathematical modelling, the experimental data presented here provide evidence that turgor-driven infection of plants by *M. oryzae* is controlled by a sensor kinase, Sln1 (Fig. 4). Once a threshold of turgor is reached, Sln1 negatively regulates the biosynthesis of melanin and production of glycerol as the appressorium nucleus enters S-phase[24]. Isotropic expansion of the pressurized appressorium ceases, and Sln1 acts through the Pkc1-dependent cell-integrity pathway to activate the Nox2–NoxR NADPH oxidase thereby recruiting septins to the appressorium pore and reorganizing F-actin to facilitate force generation and polarized growth. Sln1 also inhibits the cAMP/PKA pathway; Pkc1 acts directly on PdeH to modulate levels of cAMP, and may induce glycerol efflux through the channel protein Mip1 (Fig. 3b). The septin ring acts as a diffusion barrier to ensure the localization of

polarity determinants and regulate the polymerization of F-actin[3], recruitment of the exocyst complex[25] and activity of associated chitin and glucan synthases. Collectively, these processes lead to protrusion of a rigid penetration hypha, rupture of the rice leaf cuticle and onset of rice blast disease.

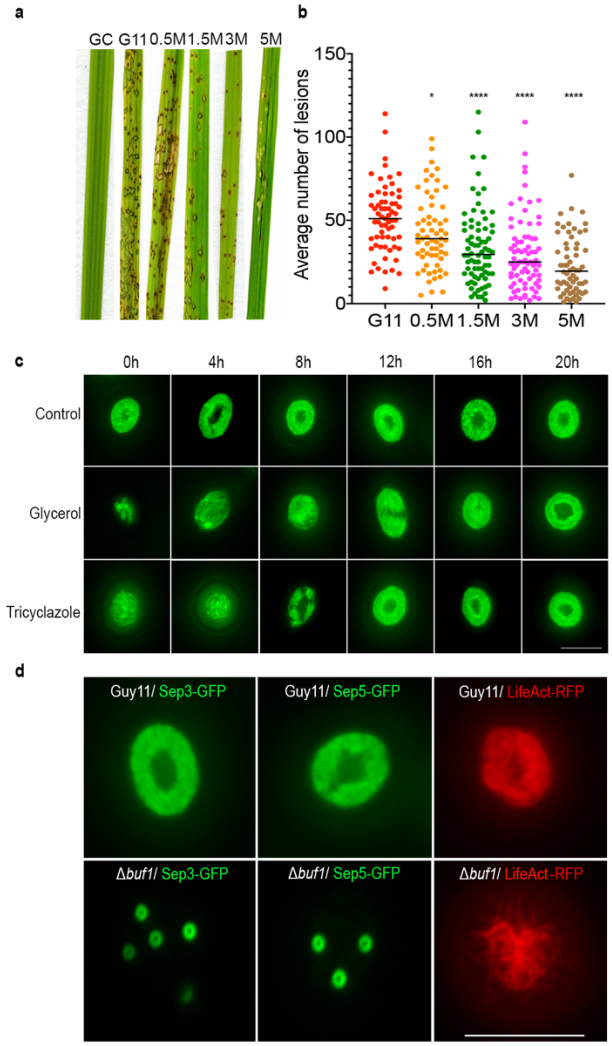

Fig. 1 Reducing appressorium turgor prevents septin-ring formation and impairs blast infection. **a**, Seedlings of rice cultivar CO-39 were inoculated with a suspension of spores of *M. oryzae* (1×10^5 conidia per ml in an aqueous solution of 0.2% gelatin) of the wild-type strain Guy11. At 5 h.p.i., seedlings were sprayed with glycerol solutions of 0.5 M, 1.5 M, 3 M and 5 M, respectively. GC, glycerol control; G11, Guy11 control. Seedlings were incubated for 5 d to observe the symptoms of blast disease. **b**, Dot plot showing the frequency of disease lesions observed in a 5-cm zone from each individual leaf harvested (60 leaves were harvested per treatment). Data are the mean and individual data points for $n = 3$ independent biological replicates. A two-tailed, unpaired Student's *t*-test with Welch correction was used for comparisons with the Guy11 control (*$P = 0.0312$, ****$P < 0.0001$). **c**, Cellular localization of Sep5–GFP at the appressorium pore of Guy11 after treatment with 1.5 M glycerol or 100 μM tricyclazole between 0 and 20 h.p.i., imaged at 24 h.p.i. Images are representative of $n = 3$ independent biological replicates. **d**, Organization of Sep3–GFP, Sep5–GFP and LifeAct–RFP in the appressorium pore of the melanin-deficient mutant Δ*buf1*. Images represent $n = 3$ independent biological replicates. Scale bars, 10 μm (**c**, **d**).

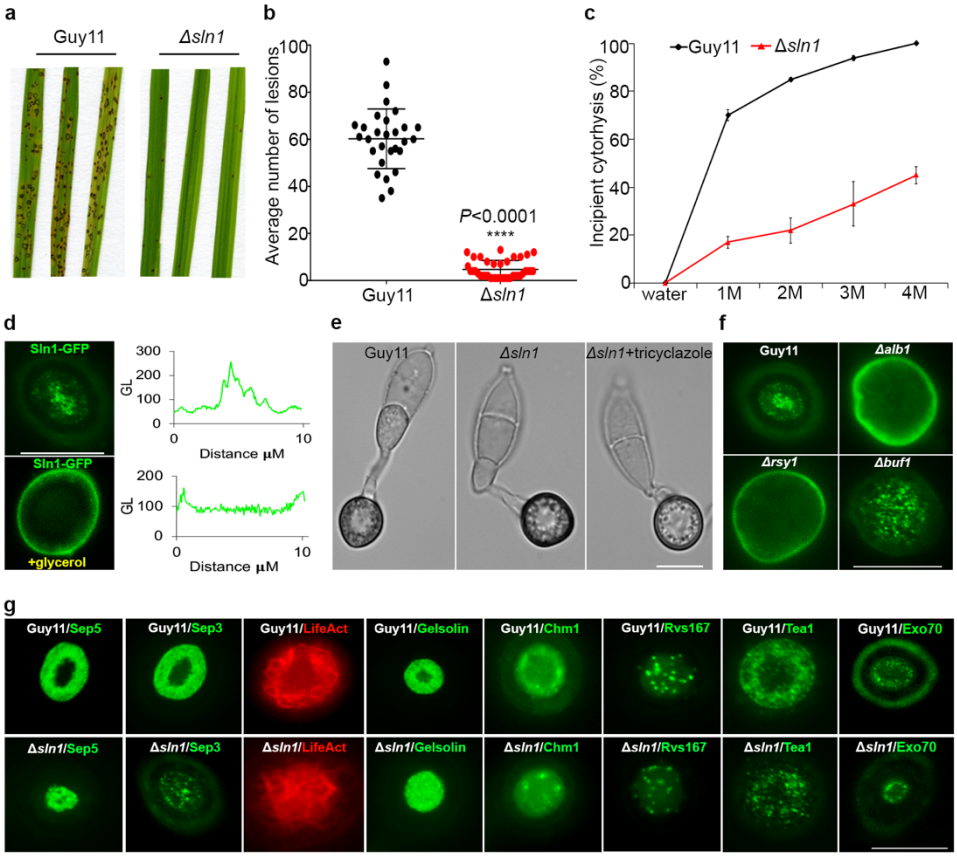

Fig. 2 Identification of the Sln1 turgor-sensing kinase in *M. oryzae*. **a**, Rice blast assay of a Δ*sln1* kinase mutant. Rice cultivar CO-39 was inoculated with a 0.2% gelatin suspension of 1 × 10^5 conidia per ml of wild-type Guy11 or the isogenic Δ*sln1* mutant, and incubated for 120 h to allow development of the symptoms of blast disease. **b**, Dot plot showing the frequency of disease lesions observed in a 5-cm zone from each individual leaf harvested (28 individual leaves were harvested per strain). Data are mean ± s.e.m. and individual data points for $n = 2$ independent biological replicates. ****$P < 0.0001$ (two-tailed, unpaired Student's *t*-test with Welch correction). **c**, Percentage of Guy11 and Δ*sln1*- mutant appressoria that undergo incipient cytorrhysis after treatment with glycerol solutions of 1.0–4.0 M. Data are mean ± s.e.m. for $n = 3$ independent experiments; 50 appressoria were counted per experiment. $P < 0.01$ for Guy11 versus 0.5 M glycerol; $P < 0.0001$ for Guy11 versus 1.5 M, 3 M and 4 M glycerol (two-tailed unpaired Student's *t*-test). **d**, Left, epifluorescence micrographs showing the cellular distribution of Sln1–GFP in appressoria at 24 h.p.i., after exposure of appressoria to 1.5 M glycerol at 5 h.p.i. Right, line-scan graphs showing Sln1–GFP fluorescence in transverse sections of individual appressoria. Images are representative of $n = 3$ independent repeats of the experiment. **e**, Micrographs of appressoria of Guy11 and a Δ*sln1* mutant to show the melanin layer. Hyper-melanization of Δ*sln1* could be reversed by exposure to tricyclazole. Images are representative of $n = 3$ independent repeats of the experiment. **f**, Sln1–GFP expression and localization in appressoria of Δ*alb1*, Δ*rsy1* and Δ*buf1* mutants at 24 h.p.i. Images are representative of $n = 3$ independent repeats of the experiment. **g**, Localization patterns of Sep3–GFP, Sep5–GFP, LifeAct–RFP, gelsolin–GFP, Chm1–GFP, Tea1–GFP and Exo70–GFP in appressorium pores of Guy11 and a Δ*sln1* mutant. Images are representative of $n = 3$ independent repeats of the experiment. Scale bars, 10 μm (**d**–**g**).

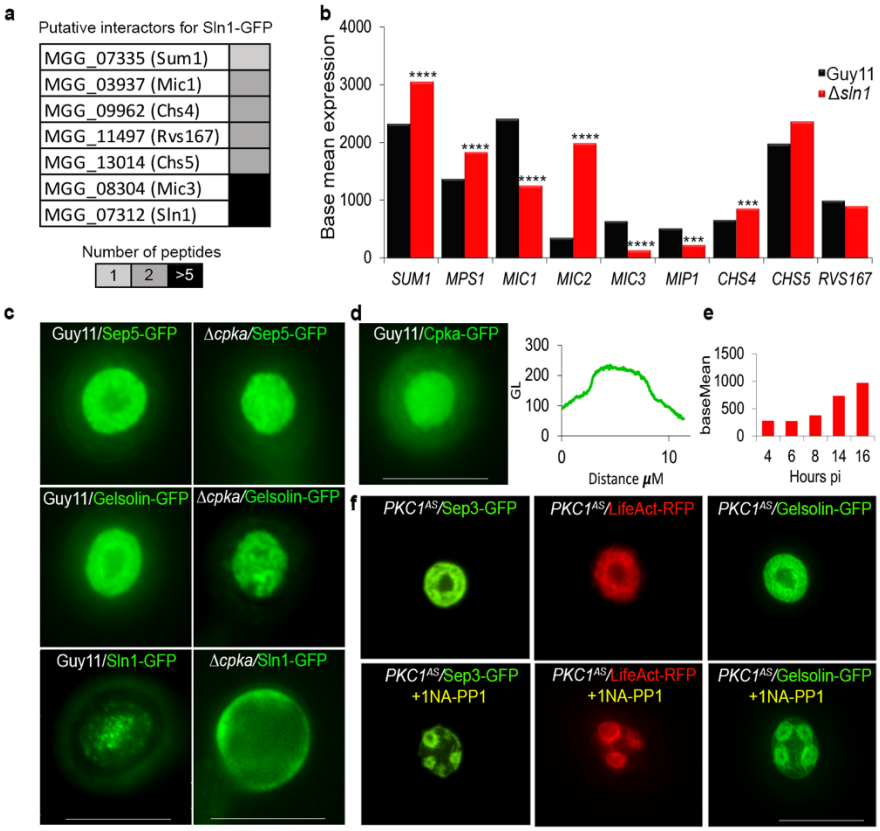

Fig. 3 Characterization of the Sln1 turgor-sensing complex in *M. oryzae*. **a**, Putative Sln1-interacting peptides were immunoprecipitated from appressorium protein extracts at 16 h.p.i. from *M. oryzae* expressing Sln1–GFP or free cytoplasmic GFP using anti-GFP antibodies, and LC– MS/MS was performed to identify unique putatively interacting peptides. Colours represent the number of identified peptides for each selected protein. **b**, Differential expression of *SUM1*, *MPS1*, *MIC1*, *MIC2*, *MIC3*, *MIP1*, *CHS4*, *CHS5* and *RVS167* in Δ*sln1*-mutant appressoria compared to Guy11 appressoria at 16 h.p.i. by RNA-seq analysis. $n = 3$ independent biological repeats of the experiment for each strain. ***$P < 0.001$,****$P < 0.0001$ (from multiple testing using the Benjamini–Hochberg method to estimate false discovery rate). **c**, Cellular localization of Sep5– GFP, gelsolin–GFP and Sln1–GFP in appressorium pores of Guy11 and a Δ*cpka* mutant at 24 h.p.i. Images are representative of $n = 3$ independent repeats of the experiment. **d**, Left, cellular distribution of Cpka–GFP in appressorium pores at 24 h.p.i. Right, line-scan graph showing Cpka– GFP fluorescence in a transverse section of an individual appressorium. Images are representative of $n = 3$ independent repeats of the experiment. **e**, Relative expression of *CPKA* from 4–24 h.p.i. during appressorium development. Data are from SuperSAGE analysis[26]. **f**, Localization of Sep3–GFP, LifeAct–RFP and gelsolin–GFP in appressorium pores of *PKC1*^{AS} mutants in the presence or absence of 1NA-PP1. Images are representative of $n = 3$ independent repeats of the experiment.

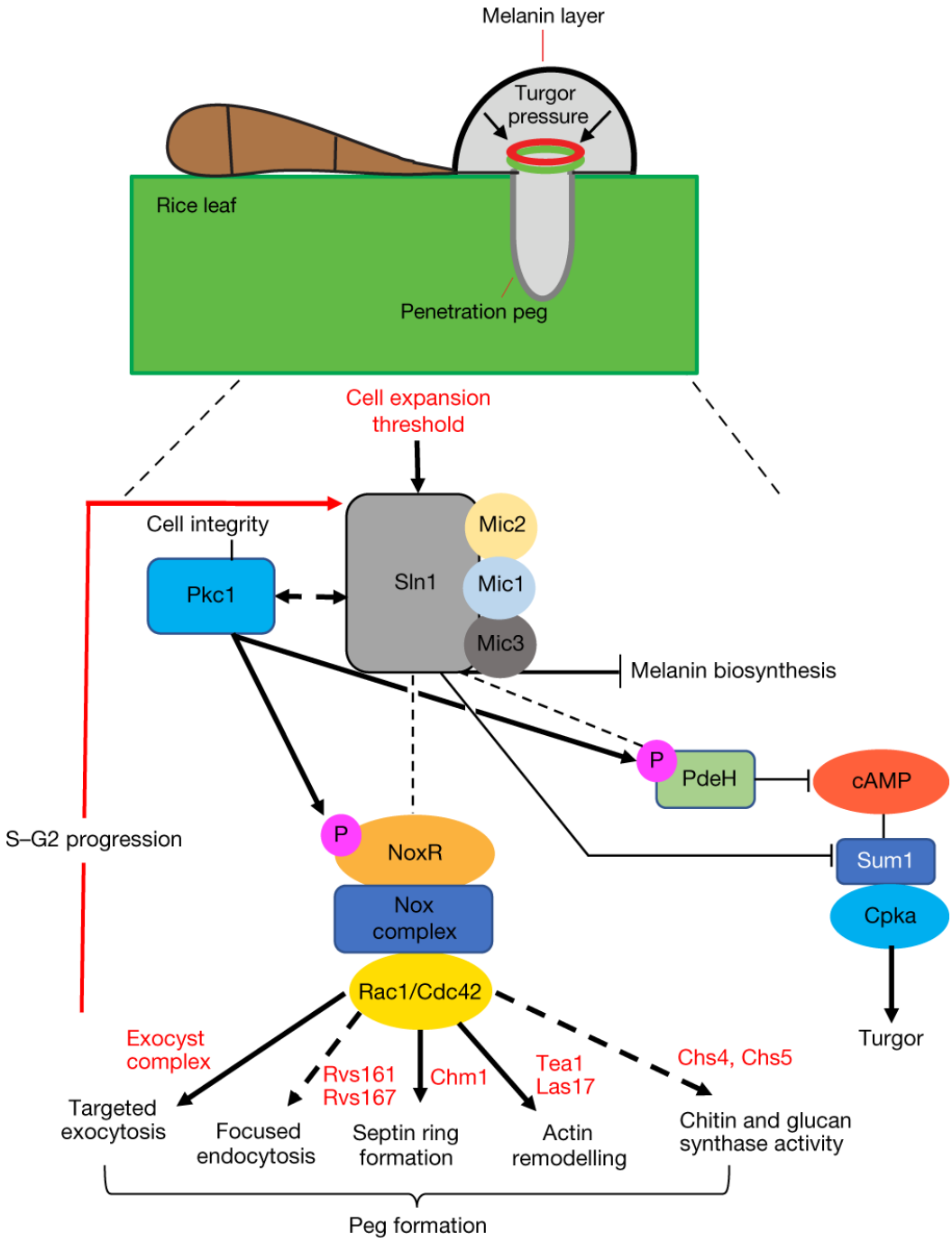

Fig. 4 Model of turgor-driven invasion of a plant cell by the rice blast fungus. The Sln1 sensor kinase responds to appressorium turgor by interaction with a set of upstream monitors of cell expansion, including the stretch-activated ion-channel proteins Mic1, Mic2 and Mic3. Once a threshold of turgor is reached, Sln1 negatively regulates melanin biosynthesis and the cAMP/PKA pathway. Pkc1 acts directly on the PdeH phosphodiesterase to modulate levels of cAMP, and also acts to control lipolysis and glycerol production. Sln1 is then necessary for recruitment of septins to the appressorium pore, which requires Pkc1 and the NADPH oxidase Nox2. Septins tether cortical F-actin to the membrane, facilitating the formation of a toroidal network of F-actin, and organizing the exocyst complex and a large family of endocytic proteins at the pore. The septin ring acts as a diffusion barrier to ensure repolarization of the penetration peg, which involves the focused polymerization of F-actin and the activity of chitin and glucan synthases. A pressure-dependent S-phase checkpoint is also triggered[22] and is necessary for the action of Sln1. Collectively, these processes lead to breaching of the rice leaf cuticle.

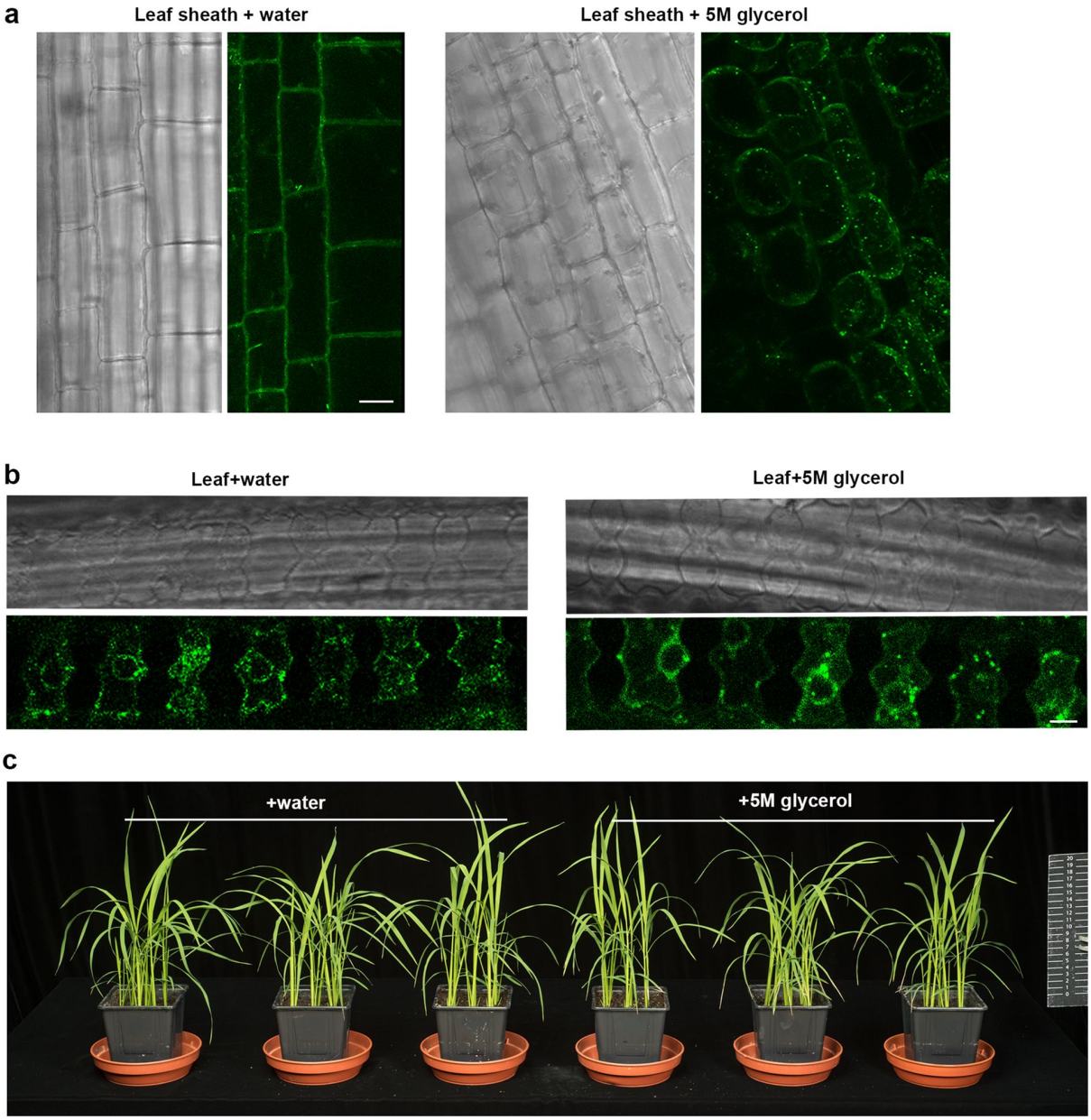

Extended Data Fig. 1. Application of glycerol to intact rice leaves does not cause cell collapse. **a,** Micrographs showing epidermal strips of a transgenic rice line that expresses the plasma-membrane marker Lti6B–GFP, treated with either water or glycerol (5 M) for 24 h. Treatment with glycerol caused cell collapse. **b,** Intact leaves from 2-week-old Lti6B–GFP transgenic rice plants were inoculated with 30-µl drops of water or 5 M glycerol and incubated for 3 days. No plasmolysis was observed; that is, glycerol was unable to cause the collapse of cells in whole plants. **c,** Rice plants were treated with water or 5 M glycerol spray and incubated for 5 days (n = 3 independent replications of the experiment). Glycerol did not have any effect on the health of the rice plant or cause any wilting confirming that no plasmolysis of rice cells from intact leaves occurs (as shown in b). Micrographs are representative of two independent replicates of the experiment. Scale bars, 20 µm (a); 5 µm (b).

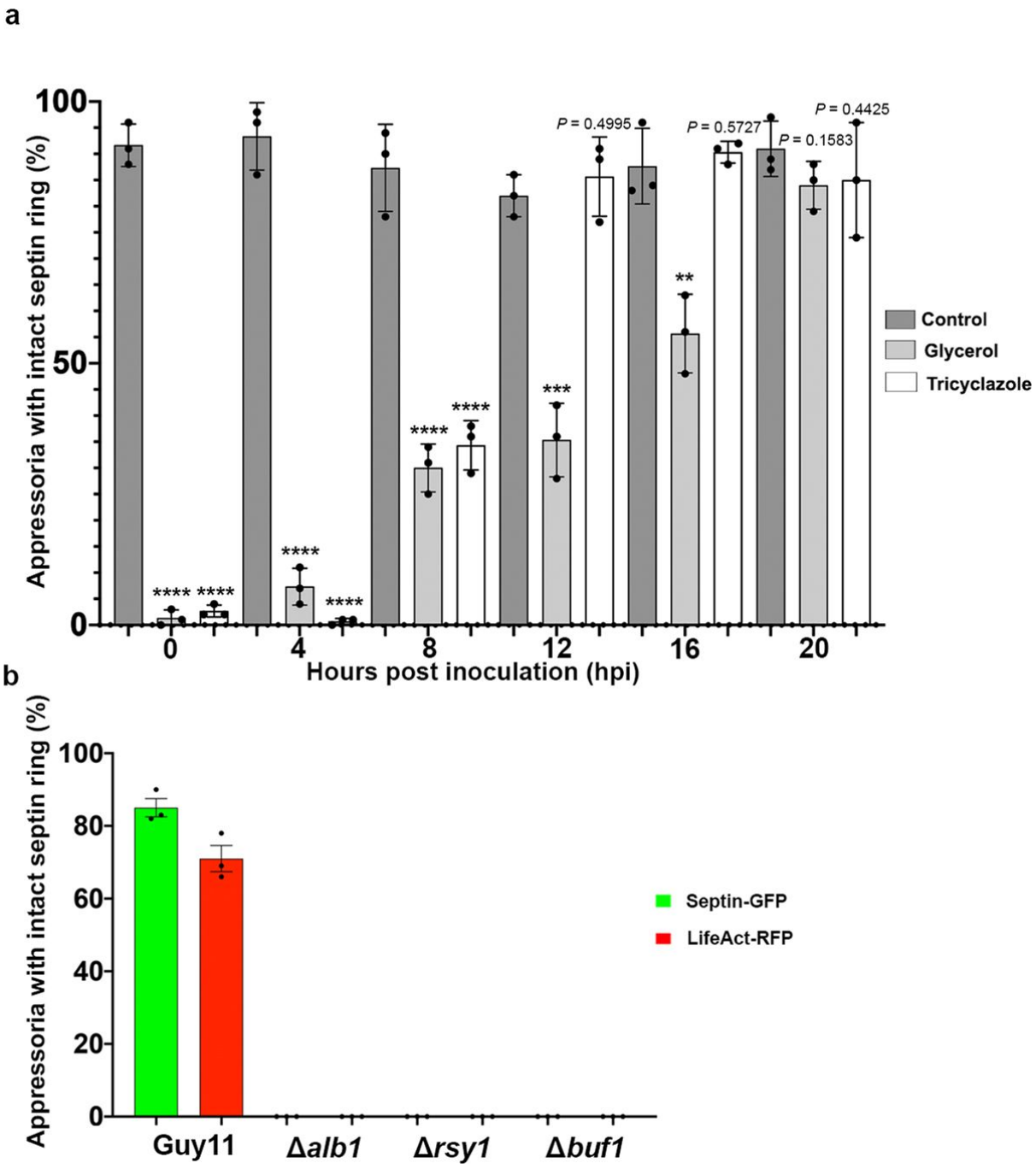

Extended Data Fig. 2. Septin organization is impaired by artificial lowering of turgor or inhibition of melanin biosynthesis. a, Percentage of appressoria that have intact septin rings after treatment with 1.5 M glycerol or 100 µM tricyclazole. Treatments were applied between 0 and 20 h.p.i and quantified at 24 h.p.i. A window of effect could thus be defined for reaching the threshold of appressorium turgor (by 16–20 h.p.i.) and for completion of melanization (by 12 h.p.i. Data are mean ± s.d. for *n* = 3 independent biological replicates; 100 appressoria were counted per replicate. ****$P < 0.0001$,***$P < 0.001$, **$P < 0.01$ (two-tailed unpaired Student's *t*-test compared to untreated Guy11 control). **b,** Percentage of appressoria that have intact septin GTPase and F-actin rings in wild-type Guy11 and the melanin-deficient mutants Δ*alb1*, Δ*rsy1* and Δ*buf1* at 24 h.p.i. Data are mean ± s.d. for *n* = 3 independent biological replicates; 100 appressoria were counted per replicate.

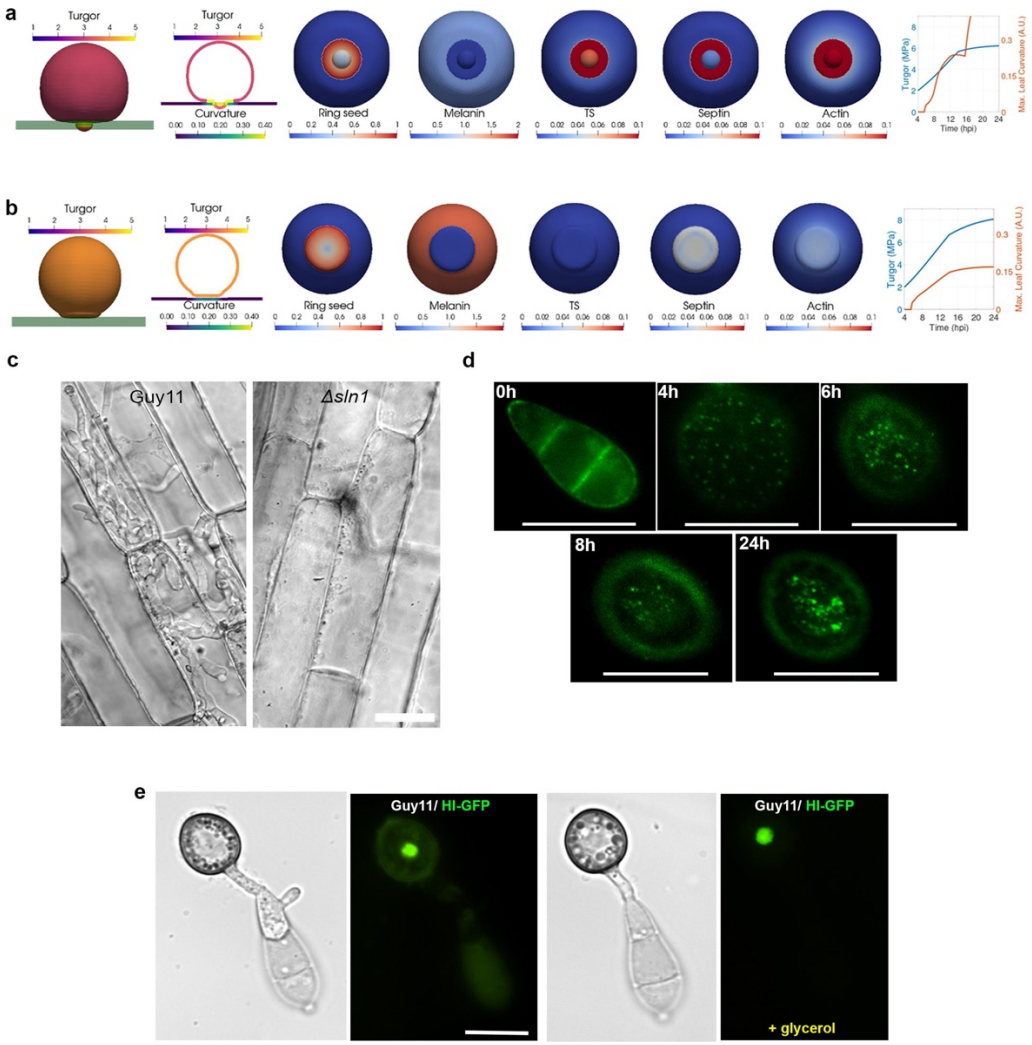

Extended Data Fig. 3. Characteristics of the Sln1 turgor-sensor kinase. a, Graphical simulation of a mathematical model for appressorium function in *M. oryzae*. The model assumes that septins are recruited to the appressorium pore at a seeded ring structure that allows the recruitment of F-actin. Melanin is recruited to the appressorium dome in proportion to increasing turgor, and excluded from the pore. A turgor sensor (TS) is recruited to the pore to modulate melanization and turgor generation, while positively regulating septin recruitment and F-actin reorganization; this results in cuticle rupture (Supplementary Video1). **b,** A mutant that lacks the turgor sensor generates excess appressorium turgor, recruits more melanin to the cell wall and prevents the recruitment of septin and F-actin to the pore; the cuticle is therefore not breached (Supplementary Video 2). **c,** Micrographs showing that the Δ*sln1* mutant is unable to invade and colonize rice tissue after 36 h.p.i. No invasive hyphae were visualized inside rice cells inoculated with Δ*sln1*. Images are representative of $n = 2$ independent biological replicates. Scale bar, 10 µm. **d,** Localization of Sln1–GFP in conidia and appressoria of *M. oryzae*. Conidia were collected from a *M. oryzae* Guy11 transformant that expresses a Sln1–GFP gene fusion, and inoculated on glass coverslips. Images were captured at 0, 4, 6, 8 and 24 h.p.i. Micrographs are representative of the distribution of Sln1–GFP at the indicated time points in $n = 3$ independent biological replications of the experiment. Scale bars, 10 µm. **e,** Epifluorescence micrographs showing that the cellular distribution of H1–GFP in appressoria at 24 h.p.i. is unaffected by exposure of appressoria to 1.5 M glycerol at 5 h.p.i. Images are representative of $n = 3$ independent biological replicates; 50 appressoria were counted per replicate. Scale bar, 10 µm.

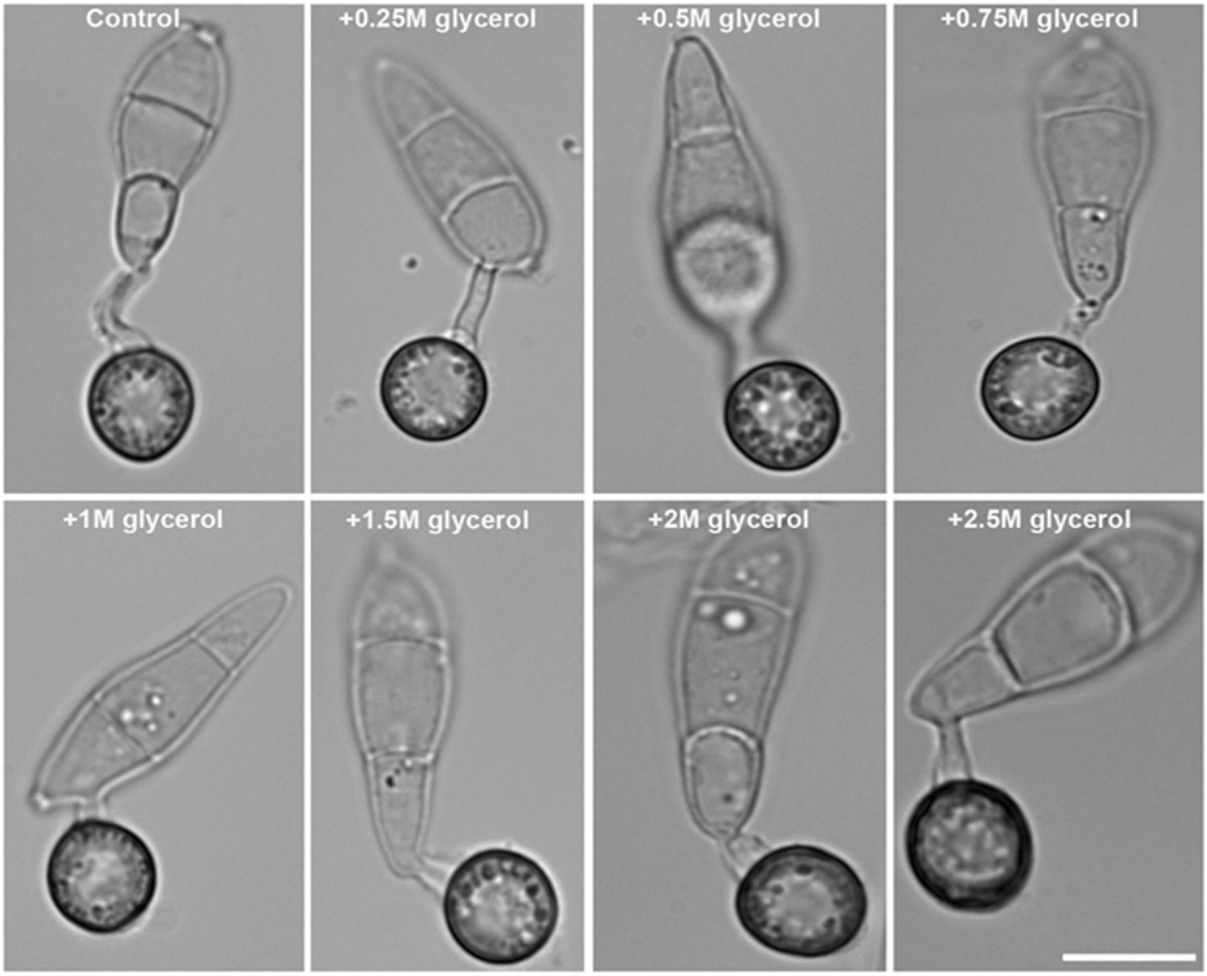

Extended Data Fig. 4. Deposition of melanin in appressoria increases in a dose-dependent manner after exposure to hyperosmotic stress. Conidia were collected from the Guy11 strain and inoculated on glass coverslips. Glycerol solutions of different concentrations (ranging from 0.25 to 2.5 M) were applied 3–4 h.p.i. and the appressoria were imaged by bright-field microscopy at 24 h.p.i. to visualize the melanin layer in the appressorium. Artificially lowering turgor by application of hyperosmotic stress led to continual melanization of the appressorium consistent with melanin biosynthesis and cell-wall deposition being turgor-dependent. Images are representative of $n = 2$ independent biological replications of the experiment. Scale bar, 10 μm.

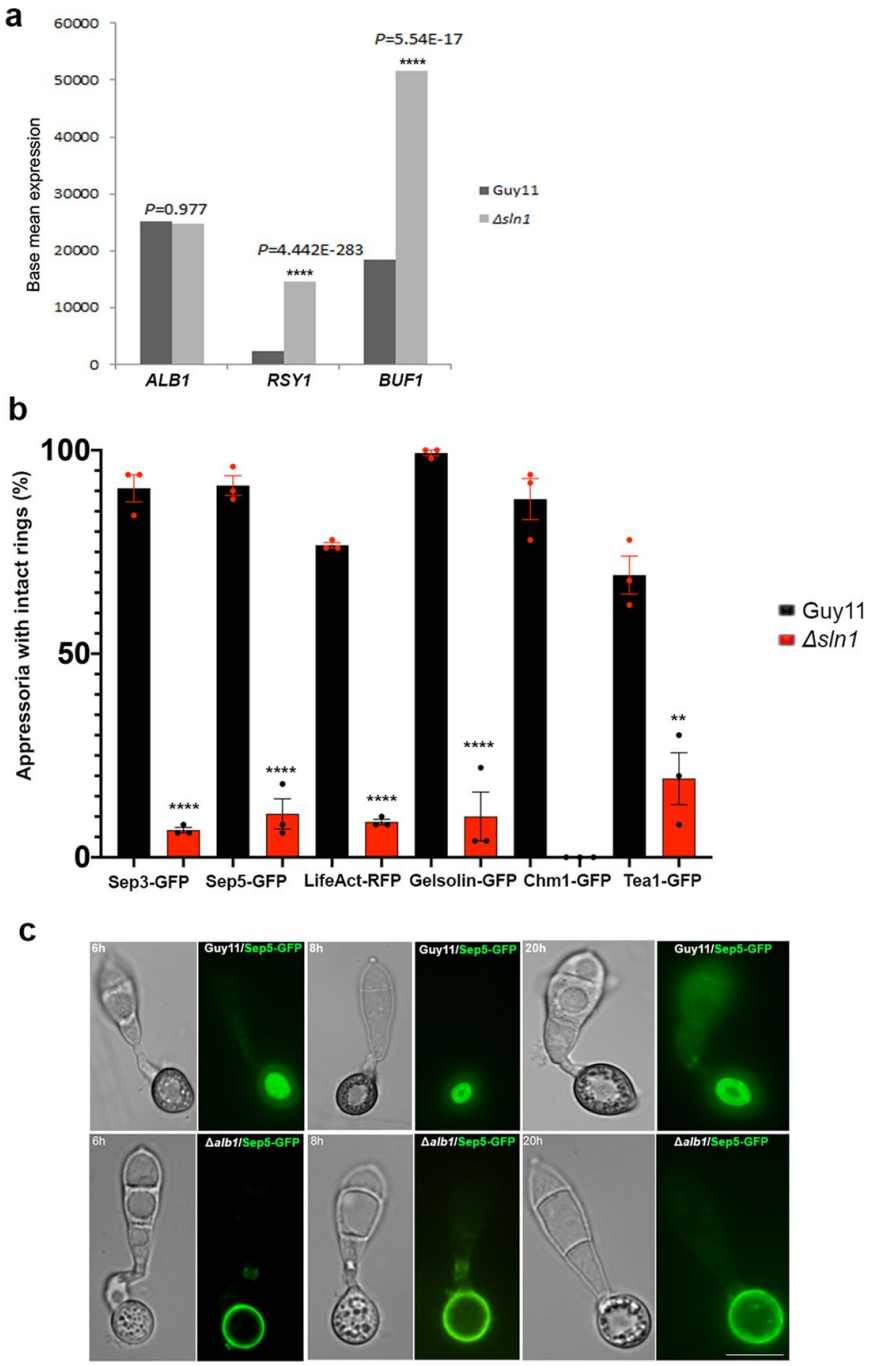

Extended Data Fig. 5. Melanin biosysnthesis and cytoskeletal organization is affected in Δ*sln1* mutants. **a,** Transcript abundance of genes that are involved in DHN-melanin biosynthesis in a Δ*sln1* mutant compared to Guy11 in appressoria at 16 h.p.i. Gene expression is represented as base mean expression from $n = 3$ three RNA-seq experiments. ****$P < 0.0001$ (two-tailed unpaired Student's *t*-test). **b,** Sln1 is required for the septin-mediated reorganization of F-actin at the appressorium pore. Conidia were collected from Guy11 transformants that express Septin3–GFP, Septin5–GFP, LifeAct–RFP, gelsolin–GFP, Chm1–GFP and Tea1–GFP gene fusions, inoculated on glass coverslips and observed by epifluorescence microscopy at 24 h.p.i. The proportion of appressoria that have intact rings was recorded. Data are mean ± s.d. for $n = 3$ independent biological replicates; 50 appressoria were counted per replicate. ****$P < 0.0001$, **$P < 0.01$ (two-tailed unpaired Student's *t*-test). **c,** Septin5–GFP is not recruited to the appressorium pore in a melanin-deficient Δ*alb1* mutant. Conidia were collected from Guy11 and Δ*alb1* transformants that express Sep5–GFP, inoculated on glass coverslips and observed by epifluorescence microscopy at 6, 8 and 20 h.p.i. The distribution of Sep5–GFP at the cell cortex or appressorium pore was recorded. Images are representative of $n = 3$ independent biological replicates. Scale bar, 10 μm.

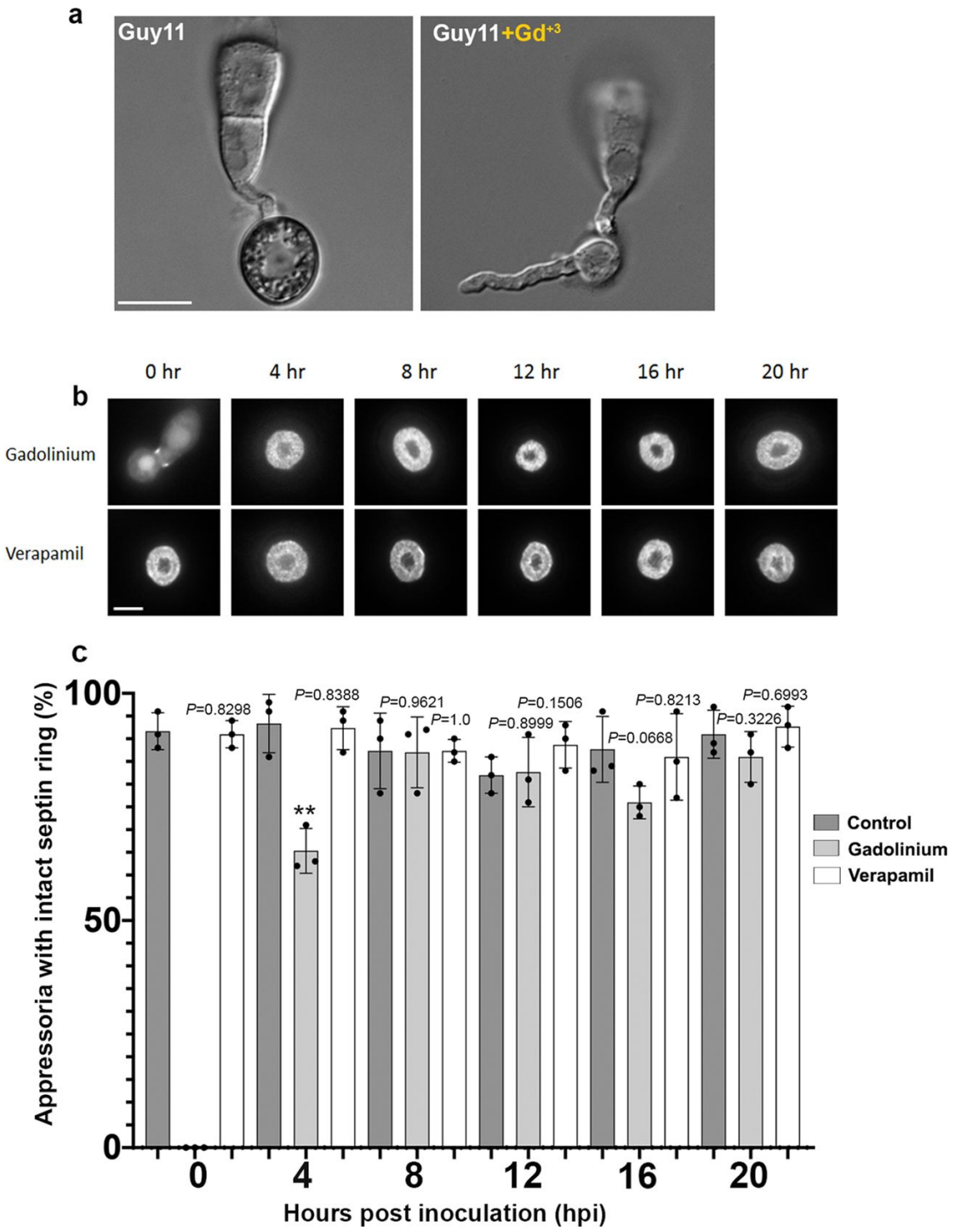

Extended Data Fig. 6. Mechanosensitive ion channels are required for appressorium formation but dispensable for septin-mediated cytoskeletal reorganization. a, Conidia were collected from Guy11 and inoculated on glass coverslips in the presence and absence of gadolinium ($Gd^{+}3$). Appressoria were imaged by bright-field microscopy at 24 h.p.i. Addition of gadolinium disrupted appressorium formation. Images are representative of $n = 3$ independent biological replications of the experiment. **b,** Micrographs showing the cellular localization of Sep5–GFP at the appressorium pore of Guy11 after treatment with gadolinium or verapamil at 0–20 h.p.i., imaged at 24 h.p.i. Images are representative of $n = 3$ independent biological replicates. Scale bars, 10 μm (a, b). **c,** Percentage of appressoria that have intact septin rings after treatment with gadolinium and verapamil. Data are mean ± s.d. for $n = 3$ independent biological replicates; 100 appressoria were counted per replicate. $^{**}P < 0.01$ (two-tailed unpaired Student's *t*-test).

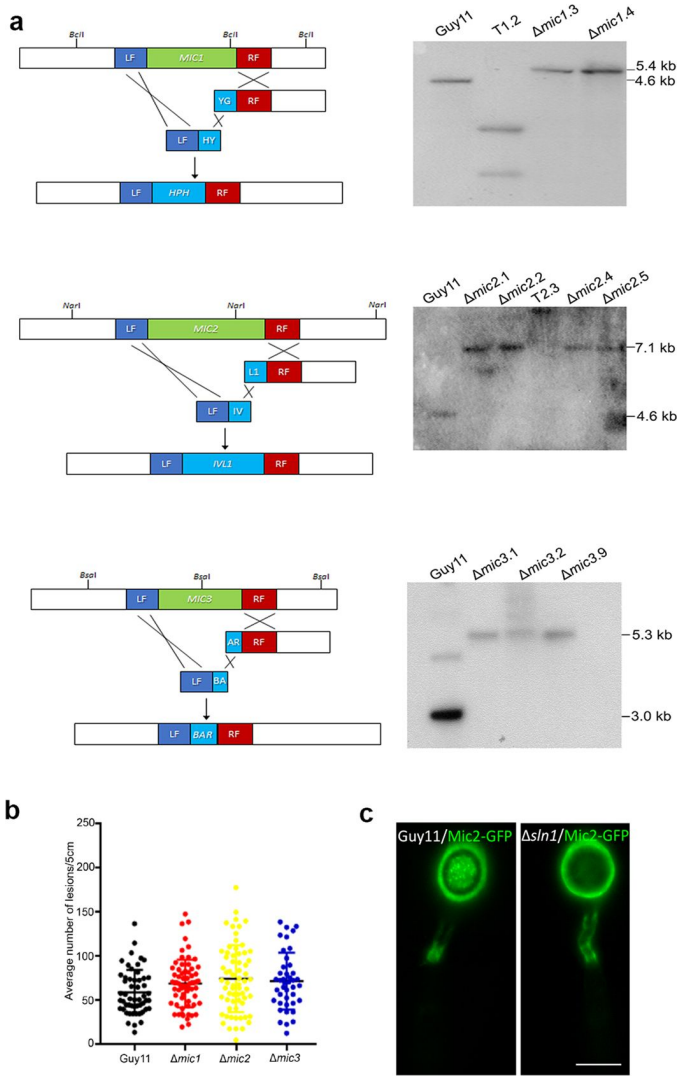

Extended Data Fig. 7. Mechanosensitive ion channels are dispensable for pathogenicity. **a**, Schematic representation of the split-marker method that was used to generate targeted deletions of genes that encode mechanosensitive ion channels, LF denotes left flank and RF denotes right flank as regions flanking the open reading frame for the gene of interest. Primers are shown in Supplementary Table 1. Deletion mutants were identified by Southern blot analysis (for gel source data of the Δ*mic1*, Δ*mic2* and Δ*mic3* gene-deletion digests for Southern blotting, see Supplementary Fig. 1a, b and c, respectively). **b**, Dot plot showing the frequency of disease lesions observed in a 5-cm zone from each individual leaf harvested per strain (60 leaves were harvested per strain). Data are the mean and individual data points for $n = 2$ independent biological replicates. Each data point represents the number of lesions on an infected rice leaf. $P > 0.01$ (two-tailed, unpaired Student's t-test with Welch-correction, compared to a Guy11 control). **c**, Micrographs showing the cellular localization of Mic2–GFP at the appressorium pore of Guy11 and Δ*sln1* at 24 h.p.i. Images are representative of $n = 3$ independent biological replicates. Scale bar, 10 μm.

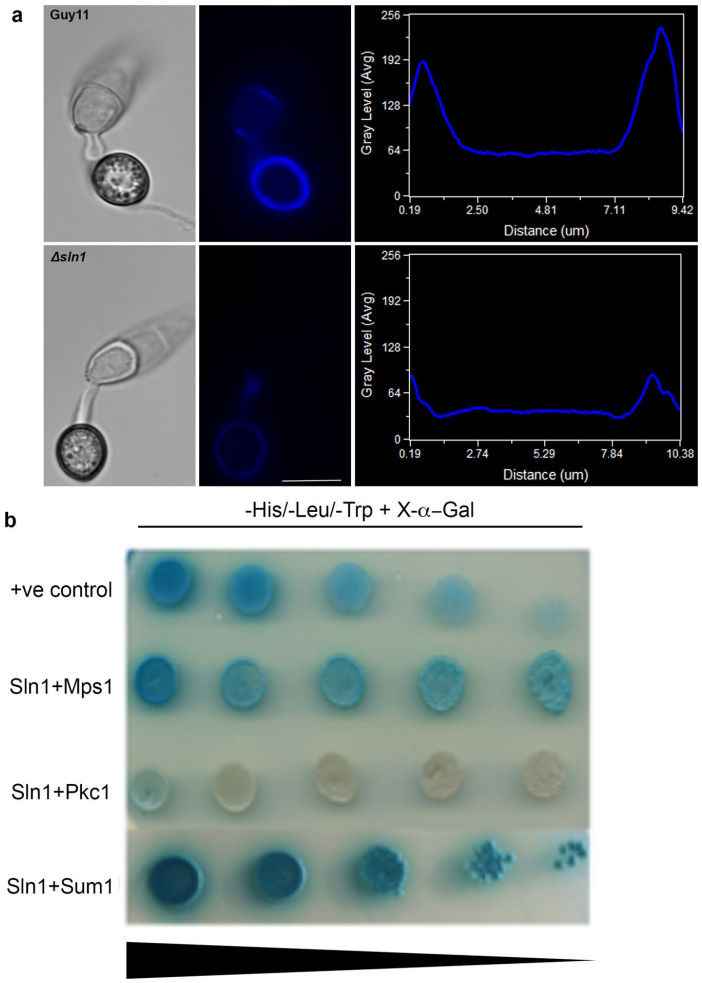

Extended Data Fig. 8. Chitin deposition in the appressorium cell wall is impaired in a Δ*sln1* mutant. a, Conidia were collected from Guy11 and the Δ*sln1* mutant and inoculated on glass coverslips to form appressoria. At 24 h.p.i., appressoria were stained with 50 μM calcofluor white for 5 min in the dark, washed and images captured by epifluorescence microscopy. Line-scan graphs represent calcofluor white fluorescence in a transverse section of an individual appressorium. Images are representative of $n = 3$ independent biological replicates. Scale bar, 10 μm. **b**, The Sln1 kinase interacts with Sum1, Pkc1 and Mps1 in a yeast two-hybrid assay. Simultaneous co-transformation of pGAD-Sln1 (prey vector) with pGBK-Mps1, pGBK-PKC and pGBK-Sum1 (bait vectors) and pGBKT7-53 and pGADT7-T (positive-control vectors) into the Y2H Gold strain resulted in the activation of three reporter genes and growth on medium-stringency medium (−Ade, −Leu, –Trp, +X-α-gal). Co-transformation also activates the expression of *MEL1*, which results in the secretion of α–galactosidase and the hydrolysis of X-α-gal in the medium, turning the yeast colonies blue. Images are representative of $n = 2$ biological replications of the experiment.

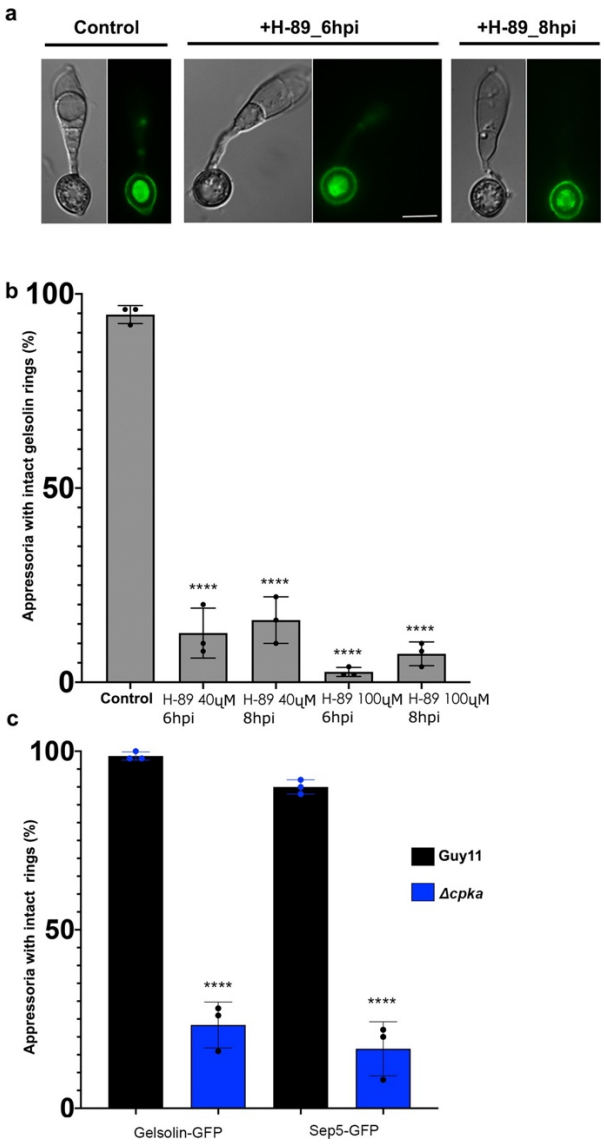

Extended Data Fig. 9. The PKA inhibitor H-89 disrupts gelsolin ring assembly. a, Micrographs showing the cellular localization of gelsolin–GFP at the appressorium pore of Guy11 after treatment with the PKA inhibitor H-89 at 6 h.p.i. and 8 h.p.i., imaged at 24 h.p.i. Images are representative of $n = 3$ independent biological replications of the experiment. Scale bar, 10 μm. **b,** Percentage of appressoria that have intact gelsolin rings after treatment with H-89. Data are mean ± s.d. for $n = 3$ independent biological replicates; 50 appressoria were counted per replicate. ****$P < 0.0001$ (two-tailed unpaired Student's *t*-test). **c,** Percentage of appressoria that have intact gelsolin and septin rings in Guy11 and the Δ*cpka* mutant. Rings were routinely smaller in Δ*cpka* than in Guy11, indicating the reduced diameter of the appressorium in the Δ*cpka* mutant. Data are mean ± s.d. for $n = 3$ independent biological replicates; 50 appressoria were counted per replicate. ****$P < 0.0001$ (two-tailed unpaired Student's *t*-test).

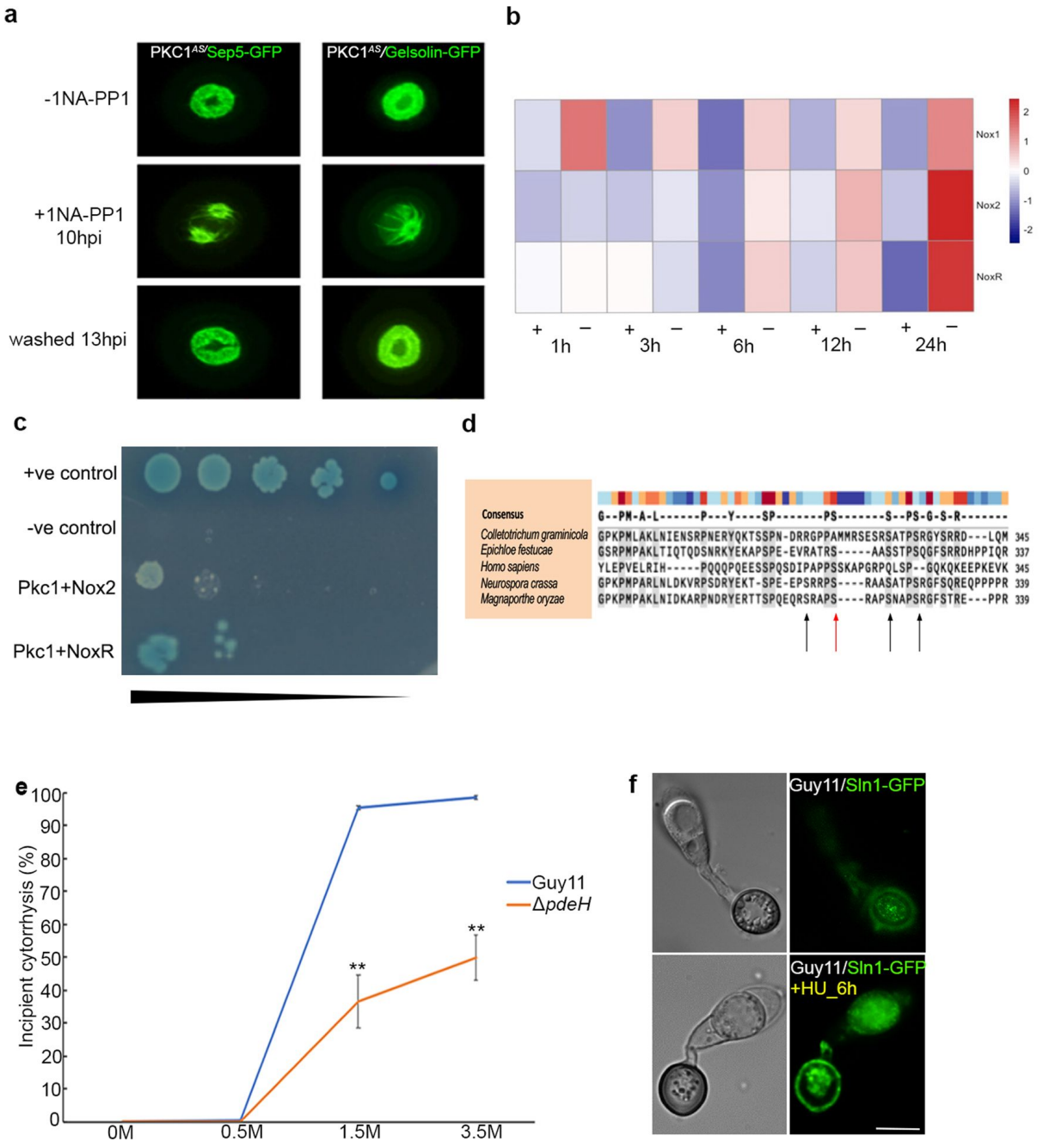

Extended Data Fig. 10. Interplay between the cell integrity and cAMP-dependent protein kinase A pathways in turgor sensing by the rice blast fungus. a, Inhibition of Pkc1 activity with 1NA-PP1 can be reversed to restore septin and gelsolin ring formation. Micrographs showing the cellular localization of Sep5–GFP and gelsolin–GFP at the appressorium pore following Pkc1 blocking at 10 h.p.i. and releasing at 13 h.p.i. Appressoria were imaged at 24 h.p.i. Images are representative of $n = 2$ replications of the experiment. **b,** Heat map showing the expression of *NOX1*, *NOX2* and *NOXR* in an RNA-seq analysis of the *PKC1*^{AS}-mutant. Mycelium was grown in CM shake cultures for 48 h in the presence or absence of 500 nM 1NA-PP1 at 1, 3, 6, 12 or 24 h.p.i. ($n = 3$ biological replications of the experiment). The full RNA-seq dataset from this study can be found at the Gene Expression Omnibus (GEO) under accession number GSE70308. **c,** Pkc1 interacts with Nox2 and NoxR in a yeast two-hybrid assay. Simultaneous co-transformation of pGBK-PKC (bait vector) and pGAD-Nox2 and pGAD-NoxR (prey vectors) into the Y2H Gold strain resulted in the activation of three reporter genes and growth on medium-stringency medium for Pkc1 and NoxR (−His, −Leu, –Trp, +X-

α-gal), and on high-stringency medium for Pkc1 and Nox2 (–His, −Leu, −Trp, −Ade, +X-α-gal). Co-transformation also activates the expression of *MEL1*, which results in the secretion of α–galactosidase and the hydrolysis of X-α-gal in the medium, turning the yeast colonies blue. Images are representative of $n = 3$ independent biological replications of the experiment. **d,** Alignment of a region of the predicted amino acid sequence of NoxR using Muscle[40]. Sequence conservation is shaded in grey, with a consensus threshold of 75%. The predicted Pkc1 phosphorylation site is marked with a red arrow and is highly conserved; black arrows indicate other potential Pkc1 phosphorylation targets based on the motif S*APS. **e,** Δ*pdeH* mutants generate excess appressorium turgor. Percentage of Guy11 and Δ*pdeH*-mutant appressoria that undergo incipient cytorrhysis after exposure to glycerol solutions of 0–3.5 M. Data are mean ± s.e.m. for $n = 3$ independent biological replicates; 50 appressoria were counted per replicate. $^{**}P < 0.01$ (two-tailed unpaired Student's *t*-test). **f,** Cellular localization of Sln1–GFP in appressorium pores of Guy11, with or without hydroxyurea (HU) added at 6 h.p.i and imaged at 24 h.p.i. Images are representative of $n = 3$ independent biological replicates. Scale bars, 10 μm.

Methods

Fungal strains, growth conditions and DNA analysis

Growth, maintenance and storage of *M. oryzae* isolates, medium composition, nucleic acid extraction and transformation were all as previously described[27]. Gel electrophoresis, restriction enzyme digestion, gel blots and sequencing were performed using standard procedures[28].

Assays of appressorium development and plant infection, quantification of melanin thickness and live cell imaging of cytoskeletal components of *M. oryzae*

Appressorium development was induced in vitro on borosilicate 18 × 18-mm glass coverslips (Thermo Fisher Scientific), adapted from a previous study[29]. A total of 50 µl of conidial suspension (5×10^4 ml^{-1}) was placed on a coverslip and incubated at 24 °C. Rice leaf sheaths were inoculated[30] to observe the development of invasive hyphae. The transgenic line expressing LTi6B was used to observe plant cell viability[31]. At the desired time points, tricyclazole (100 µM), an agent that inhibits melanin biosynthesis, was added to *M. oryzae* and infection-related development assayed. Glycerol was used at a final concentration of 1.5 M for coverslip assays unless otherwise stated, and 1–5 M for plant spraying, and samples were incubated at 24 °C. Gadolinium (100 µM) and verapamil (100 µM) were added at the indicated times to evaluate their effect on infection-related development (0–20 h). To determine the thickness of the melanin layer of the appressorium, appressoria were sampled at random intervals at the cell cortex. Development of appressoria was observed using an IX81 motorized inverted microscope (Olympus) and images were captured using a Photometrics CoolSNAP HQ2 camera (Roper Scientific), under control of the Metamorph software package (MDS Analytical Technologies). Datasets were compared using an unpaired Student's *t*-test.

Generation of GFP fusion plasmids

DNA sequences were retrieved from the *M. oryzae* database (http://fungi.ensembl.org/Magnaporthe_oryzae/Info/Index) and used to design primers (Supplementary Table 1). In-Fusion cloning based on in vitro homologous recombination was performed to generate Sln1–GFP and Cpka–GFP, using a commercial kit (In-Fusion Cloning kit; Clontech Laboratories). The primers used are shown in Supplementary Table 1. Sln1–GFP, Cpka–GFP and Mic2–GFP were inserted as EcoRI/HindIII fragments into a modified Strataclone (Stratagene) vector containing the *BAR* gene that confers bialophos (BASTA) resistance[32]. In all cases, several independent *M. oryzae* transformants were first screened for consistency of the fluorescent signal and a representative transformant was then selected for further analysis. Three independent experiments were performed in each case unless otherwise stated.

Targeted gene deletion of *MIC1*, *MIC2* and *MIC3* in *M. oryzae*

Targeted gene replacement of *M. oryzae MIC1*, *MIC2* and *MIC*3 was performed using the split marker strategy[6]. To amplify the split *HPH*, *IVL1*or *BAR* templates, the primers used were M13 (forward) with HY/ VL/BA and M13 (reverse) with YG/IV/AR, as described[33]. *M. oryzae* mechanosensitive-ion-channel genes that contain the pfam

domain (PF00924) were aligned with *Schizosaccharomyces pombe*, *Aspergillus nidulans* and *Neurospora crassa* (*Saccharomyces cerevisiae* and *Candida albicans* do not have genes with this domain). The sequence data for each mechanosensitive-ion-channel gene in *M. oryzae* were retrieved from the *M. oryzae* genome database at https://fungi.ensembl.org/Magnaporthe_oryzae/Info/Annotation/) and used to design specific primers (see Supplementary Table 1). Either Guy11 or the Δ*ku70* (*KU70* is also known as *YKU70*) mutant[33] was transformed with the deletion cassette for each gene fusion; *Mic1:hph*, *Mic2:ivl1* and *Mic3:bar*(2 μg of DNA for each flank). Transformants were selected in the presence of either hygromycin B (200 μg ml^{-1}), sulfonylurea (50 μg ml^{-1}) or bialophos (50 μg ml^{-1}) and were routinely screened and assessed using Southern blotting.

Co-immunoprecipitation experiments and LC–MS/MS analysis

Total protein was extracted from lyophilized *M. oryzae* appressoria (generated on borosilicate 18 × 18-mm glass coverslips (Thermo Fisher Scientific)) at 16 h.p.i., collected using a razor blade and snap-frozen in liquid nitrogen. *M. oryzae* strains that express Sln1–GFP and ToxA–GFP (control) were co-immunoprecipitated using the GFP-Trap protocol according to the manufacturer's instructions (ChromoTek). Preparation of peptides for LC–MS/MS was performed as follows. Proteins were separated by SDS–PAGE. Gels were cut into slices (5–10 mm) and proteins contained within gel slices were prepared for LC–MS/MS as described previously[34]. LC–MS/MS analysis was performed with an Orbitrap Fusion trihybrid mass spectrometer (Thermo Fisher Scientific) and a nanoflow high-performance liquid chromatography (HPLC) system (Dionex Ultimate3000, Thermo Fisher Scientific), as described previously[35] but with the following differences: MS/MS peak lists were exported in the Mascot generic file format using Discoverer v2.2 (Thermo Fisher Scientific). The database was searched with Mascot v.2.3 (Matrix Science), with the following differences: (1) the database searched with Mascot v.2.3 (Matrix Science) was the *M. oryzae* protein database with the inclusion of sequences of common contaminants such as keratins and trypsin; (2) carbamidomethylation of cysteine residues was specified as a fixed modification, and oxidized methionine was allowed as a variable modification. The other Mascot parameters used were as follows: (1) mass values were monoisotopic and the protein mass was unrestricted; (2) the peptide mass tolerance was 5 ppm and the fragment mass tolerance was 0.6 Da; (3) two missed cleavages were allowed with trypsin. All Mascot searches were collated and verified with Scaffold (Proteome Software), and the subset database was searched with the Mascot server v.2.4.1 (Matrix Science). Accepted proteins passed the following threshold in Scaffold: 95% confidence for protein match and minimum of two unique peptide matches with 95% confidence.

Yeast two-hybrid analysis

In-Fusion Cloning based on in vitro homologous recombination was performed to generate vectors that express Sln1, Nox1, Nox2 and NoxR in the pGADT7 prey vector, and Mps1, Pkc1[20] and Sum1 in the pGBKT7 bait vector. Genes were amplified from *M. oryzae* cDNA derived from mycelium grown on liquid Complete Medium (CM) using primers with a 15-bp overhang and a restriction site complementary to the target vector (Supplementary Table 1). Fragments were cloned into pGBKT7 and pGADT7

plasmids and linearized by digestion with BamHI and EcoRI. Yeast two-hybrid assays using pGADT7- or pGBKT7-based constructs (Clontech) were performed according to the manufacturer's instructions (MATCHMAKER Gold Yeast Two-Hybrid System).

Comparative RNA-seq analysis

Total RNA was extracted from appressoria of the wild-type strain Guy11 and Δ*sln1* null mutant at 16 h.p.i., which were developed on hydrophobic coverslips using the RNeasy Plant Mini Kit for Total RNA extraction (Qiagen). RNA-seq libraries were then prepared from 5 µg of total RNA with the Illumina TruSeq RNA Sample Preparation Kit (Agilent) according to the manufacturer's instructions. Libraries were sequenced using the Illumina HiSeq 2500 platform. Reads were aligned against version 8.0 of the *M. oryzae* genome using TopHat software and analysis of the data was performed using DESeq through moderated $\log_2$-transformed fold-change values (mod_lfc)[36,37]. Transcript abundances for each gene and adjusted *P* values and transcript abundance were determined as previously described[38].

Protein extraction and phosphoproteomic enrichment

Mycelium of the *M.oryzae PKC1*^{AS} mutant and Guy11 was prepared from CM shake cultures (125 r.p.m.) at 24 °C for 48 h. Mycelium was filtered through miracloth (Calbiochem), divided and treated with 1NA-PP1 at a final concentration of 500 nM for 4 h. An untreated control was also prepared at the same time point. Mycelium was then filtered, washed in distilled water and frozen in liquid nitrogen. Frozen tissue was ground to a fine powder in liquid nitrogen, resuspended in extraction buffer (8 M urea, 150 mM NaCl, 100 mM Tris pH 8, 5 mM EDTA, 1 µg ml^{-1} aprotinin, 2 µg ml^{-1} leupeptin) and mechanically disrupted (8 min, 1,000 r.p.m.) in a 30-ml Potter-Elvehjem homogenizer incubated on ice[22]. The homogenate was then fractionated by centrifugation for 30 min at 10,000*g* (Sorvall SW34 rotor). The supernatant was removed and then centrifuged for 60 min at 100,000*g* (Sorvall T-647.5 rotor) to separate the cytosolic (supernatant) and microsomal (pellet) fractions. The microsomal pellet was then resuspended in extraction buffer. For phosphopeptide enrichment, sample preparation started with 1–3 mg of cytosolic or microsomal protein extract (confirmed by Bradford assay) dissolved in bicarbonate buffer containing 8 M urea. First, protein extracts were reduced with 5 mM tris(2-carboxyethyl)phosphine (TCEP) for 30 min at 30 °C with gentle shaking, followed by alkylation of cysteine residues with 40 mM iodoacetamide at room temperature for 1 h. Samples were diluted to a final concentration of 1.6 M urea with 50 mM ammonium bicarbonate and digested overnight with trypsin (Promega; 1:100 enzyme to substrate ratio). Peptide digests were purified using C18 SepPak columns (Waters) as described[39]. Phosphopeptides were enriched using titanium dioxide (TiO_2; GL Science) with phthalic acid as a modifier[22]. Finally, phosphopeptides were eluted by a pH shift to 10.5 and immediately purified using C18 microspin columns (The Nest Group; loading capacity of 5–60 µg). After purification, all samples were desiccated in a speed-vac, stored at −80 °C and resuspended in 2% acetonitrile with 0.1% trifluoroacetic acid before mass-spectrometry analysis[22].

Mass-spectrometry analysis of phosphopeptide-enriched samples

LC–MS/MS analysis was performed using an Orbitrap Fusion trihybrid mass spectrometer (Thermo Fisher Scientific) and a nanoflow ultra-high-performance liquid

chromatography (UHPLC) system (Dionex Ultimate 3000, Thermo Fisher Scientific). Peptides were trapped on a reverse-phase trap column (Acclaim PepMap, C18 5 µm, 100 µm × 2 cm, Thermo Fisher Scientific). Peptides were eluted in a gradient of 3–40% acetonitrile in 0.1% formic (solvent B) acid over 120 min, followed by a gradient of 40–80% B over 6 min at a flow rate of 200 nl min^{-1} at 40 °C. The mass spectrometer was operated in positive-ion mode with a nano-electrospray ion source with ID 0.02-mm fused silica emitter (New Objective). A voltage of 2,200 V was applied via platinum wire held in PEEK T-shaped coupling union with the transfer capillary temperature set to 275 °C. The Orbitrap mass spectrometry scan resolution of 120,000 at 400 *m*/*z*, range 300–1,800 *m*/*z*was used, and the automatic gain control was set to 2×10^5 and the maximum injection time to 50 ms. In the linear ion trap, MS/MS spectra were triggered using a data-dependent acquisition method, with 'top speed' and 'most intense ion' settings. The selected precursor ions were fragmented sequentially both in the ion trap using collision-induced dissociation (CID) and in the higher-energy collisional dissociation (HCD) cell. Dynamic exclusion was set to 15 s. The charge state allowed between 2+ and 7+ charge states to be selected for MS/MS fragmentation.Peak lists in the format of Mascot generic files (.mgf files) were prepared from raw data using the MSConvert package (Matrix Science). Peak lists were searched on Mascot server v.2.4.1 (Matrix Science) against either the *Magnaporthe oryzae* (isolate 70-15, v.8) database, or an in-house contaminants database. Tryptic peptides with up to two possible miscleavages and the charge states +2, +3, +4 were allowed in the search. The following modifications were included in the search: oxidized methionine; phosphorylation on serine, threonine, or tyrosine as a variable modification; and carbamidomethylated cysteine as a static modification. Data were searched with a monoisotopic precursor and fragment-ions mass tolerance set at 10 ppm and 0.6 Da, respectively. Mascot results were combined in Scaffold v.4 (Proteome Software) and exported in Excel (Microsoft Office)[22].

Statistical analysis

All experiments were conducted with technical and biological replicates at an appropriate sample size that was estimated on the basis of our previous experience. No statistical methods were used to predetermine sample size. No methods of randomization were applied but blinding was applied to the data on disease symptoms, which are shown in Fig. 1b. All experiments were replicated independently at least once, as indicated in each figure legend. Dot plots were routinely used to show individual data points for each experimental observation, and bar graphs, where shown, also contained individual data points for each experimental replicate. Statistical analyses were performed using GraphPad Prism 8 or Microsoft Excel. *P* values <0.05 were considered significant; $*P < 0.05$, $**P < 0.01$, $***P < 0.001$, $****P < 0.0001$. *P* values >0.05 were considered non-significant and exact values are shown where appropriate. The sample sizes and statistical tests used are stated in each figure legend.

Data availability

All strains generated and datasets analysed during the current study, including codes and algorithms, are available either in public repositories as stated, or from the corresponding author on reasonable request.

Supplementary Table S1. DNA oligonucleotide primers used in this study

Primer name	Primer sequence (5'-3')
Mic150.1F	AGTAAATTTAGAAATCACAGCGCT
Mic150.1R	GTCGTGACTGGGAAAACCCTGGCGCTCCCACACTCGGCTTAGTATATC
Mic130.1F	TCCTGTGTGAAATTGTTATCCGCTATGAAAGATGAGAGGAGATGAAAT
Mic130.1R	AACCCCGCTGGATAATGCTTTTTC
Mic250.1F	GGCGATCATGTTTCTTTAGATGAC
Mic250.1R	GTCGTGACTGGGAAAACCCTGGCGCTTTAAAGAACAGTCCTCGTCGCC
Mic230.1F	TCCTGTGTGAAATTGTTATCCGCTGCTTGTAGCCAAGGCGGCTTCCGC
Mic230.1R	CAGCAGGAAGATACGTTCAGATAT
Mic350.2F	GACACGAGATATTGTCACAGTGTA
Mic350.1R	GTCGTGACTGGGAAAACCCTGGCGGTTTGCTGGCTGTCGATGGGATAA
Mic330.1F	TCCTGTGTGAAATTGTTATCCGCTAGTGCTGTTGTATGAGGAGGGGAG
Mic330.1R	TTGTAGCCGAACTCGGCCGAGTCG
Mic2F	TGCAGCCCAATGTGGAATTCATCCATGAGGGTGGAGTACTCTGA
Mic2R	GTAATAACCTGCTGAGCCCGGCTT
GFP_Mic2	TCAGCAGGTTATTACATGGTGAGCAAGGGCGAGGAGCTG
Sln1F	TGCAGCCCAATGTGGAATTCCAGATCGCATCGACCGCAGAAGAG
Sln1R	CGTCGCCACAGCAGCACCGTTCAT
GFP_Sln1	GCTGCTGTGGCGACGATGGTGAGCAAGGGCGAGGAGCTG
TrpCR	TCGACGGTATCGATAAGCTTAGTGGAGATGTGGAGTGGGCGCTTA
Sln1_DT7F	GGAGGCCAGTGAATTCATGAGGATCGCCATCCGCGAGCAG
Sln1_DT7R	CGAGCTCGATGGATCCTCACGTCGCCACAGCAGCACC
Sum1_KT7F	CATGGAGGCCGAATTCATGTCGGCCAGCGGCTTCACCAGT
Sum1_KT7R	GCAGGTCGACGGATCCTTAGGCAGCCTGTAGTGGATCCAT

CpkaF	TGCAGCCCAATGTGGAATTCAGTCTGTGGATGGATGAAAGGTTG
CpkaR	GAATCCAGGGAACAAATTCCCGTA
GFPF_cpka	TTGTTCCCTGGATTCATGGTGAGCAAGGGCGAGGAGCTG
Nox1_Pgadt7F	GGAGGCCAGTGAATTCATGTCGGTCGGAGAGTTCTTGGCT
Nox1_Pgadt7R	CGAGCTCGATGGATCCCTAGAAATGCTCCTTCCAGAAGCG
Nox2_Pgadt7F	GGAGGCCAGTGAATTCATGTCTGGATACGGCTACGGAGGA
Nox2_Pgadt7R	CGAGCTCGATGGATCCCTAGAAATTCTCCTTGCCCCATAC
NoxR_Pgadt7F	GGAGGCCAGTGAATTCATGTCGCTCAAGCAGGAGATAGAA
NoxR_Pgadt7R	CGAGCTCGATGGATCCTCATGCATCCTGAATCCAAACCT

Supplementary Table S2. Pkc1 phosphorylation targets.

Summary of In vivo Phosphorylation Sites of potential PKC targets by LC-MS/MS Analysis [1.]						Number of Spectra			
Protein identifier	Description	Phosphorylation Site	Peptide Sequence	Highest Probability	Highest Mascot Ion Score	PKCas mock	PKCas 1N-PP	Guy11 mock	Guy11 1N-PP
MGG_05280	NADPH oxidase regulator NoxR	S321	(R)SRAPsRAPSNAPSR(G)	91.50%	18.6	2	0	0	0
MGG_08304	mechanosensitive ion channel family protein	S780	(R)RGPsVVIDHGPDMFQDVYGSR(R)	99.70%	25.1	1	0	0	1
		S828	(R)AAEHTIQPPMHSPSsPGIER(T)	99.70%	34.7	0	0	3	7
MGG_03937	serine/threonine protein kinase	S24	(R)MGFMPINGGRGsEEEADIPLSTIR(T)	99.70%	49.7	2	1	5	13
MGG_06726	septin like spn2	S314/S318	(K)QLLALKDPSAQGHSSRPISPAAER(E)	99.70%	34	2	0	0	10
MGG_05664	phosphodiesterase	S883	(R)HRGASPPLSAADTAG(-)	99.70%	33.2	4	1	6	4
MGG_09869	Swi6	S276	(K)ARFDsPGPR(G)	99.70%	21.6	1	0	1	1
		S290	(R)NGPTRAPsFQR(Q)	97.40%	16.1	0	0	1	0
MGG_08463	Swi4	S448/449/450	(R)[sss]PFAPESAR(R)	99.70%	46.7	5	2	5	4
		S123	LRPIFEFSPGPDsPPPAPR	99.70%	58.7	13	12	27	25
MGG_00883	Bck1	S443/445	(R)GARQsPsDLGDNSAGTDSPVSAR(D)	99.70%	65.5	3	2	9	7
		T418/S724	(R)NAPAPPVAPSAtLNRVNsLMTGQR(R)	89.40%	21.2	1	0	2	0

[1.] Mycelium from Guy11 and *pkc1*^{AS} was grown and treated, with or without 500 nM 1NA-PP1 for 4 h. Proteins were extracted, (phospho)-peptides were enriched using titanium dioxide and injected onto the mass spectrometer. The table summarises some of the Pkc1 targets, the phosphorylation site(s) and their corresponding mascot scores >18, n=3.

1. Talbot, N. J. On the trail of a cereal killer: exploring the biology of *Magnaporthe grisea*. *Annu. Rev. Microbiol*. **57**, 177–202 (2003).
2. Ryder, L. S. & Talbot, N. J. Regulation of appressorium development in pathogenic fungi. *Curr. Opin. Plant Biol*. **26**, 8–13 (2015).
3. Dagdas, Y. F. et al. Septin-mediated plant cell invasion by the rice blast fungus, *Magnaporthe oryzae*. *Science* **336**, 1590–1595 (2012).

4. Pennisi, E. Sowing the seeds for the ideal crop. *Science* **327**, 802–803 (2010).
5. Fisher, M. C. et al. Emerging fungal threats to animal, plant and ecosystem health. *Nature* **484**, 186–194 (2012).
6. Islam, M. T. et al. Emergence of wheat blast in Bangladesh was caused by a South American lineage of *Magnaporthe oryzae*. *BMC Biol*. **14**, 84 (2016).
7. Inoue, Y. et al. Evolution of the wheat blast fungus through functional losses in a host specificity determinant. *Science* **357**, 80–83 (2017).
8. de Jong, J. C. MCCormack, B. J., Smirnoff, N. & Talbot, N. J. Glycerol generates turgor in rice blast. *Nature* **389**, 244–245 (1997).
9. Chumley, F. G. & Valent, B. Genetic-analysis of melanin-deficient, nonpathogenic mutants of *Magnaporthe grisea*. *Mol. Plant Microbe Interact*. **3**, 135–143 (1990).
10. Ryder, L. S. et al. NADPH oxidases regulate septin-mediated cytoskeletal remodeling during plant infection by the rice blast fungus. *Proc. Natl Acad. Sci. USA* **110**, 3179–3184 (2013).
11. Wilson, R. A. & Talbot, N. J. Under pressure: investigating the biology of plant infection by *Magnaporthe oryzae*. *Nat. Rev. Microbiol*. **7**, 185–195 (2009).
12. Tao, W., Deschenes, R. J. & Fassler, J. S. Intracellular glycerol levels modulate the activity of Sln1p, a *Saccharomyces cerevisiae* two-component regulator. *J. Biol. Chem*. **274**, 360–367 (1999).
13. Dixon, K. P., Xu, J.-R., Smirnoff, N. & Talbot, N. J. Independent signaling pathways regulate cellular turgor during hyperosmotic stress and appressorium-mediated plant infection by *Magnaporthe grisea*. *Plant Cell* **11**, 2045–2058 (1999).
14. Zhang, H. et al. A two-component histidine kinase, *MoSLN1*, is required for cell wall integrity and pathogenicity of the rice blast fungus, *Magnaporthe oryzae*. *Curr. Genet*. **56**, 517–528 (2010).
15. Motoyama, T. et al. Involvement of putative response regulator genes of the rice blast fungus *Magnaporthe oryzae* in osmotic stress response, fungicide action, and pathogenicity. *Curr. Genet*. **54**, 185–195 (2008).
16. Bahn, Y. S., Kojima, K., Cox, G. M. & Heitman, J. A unique fungal two-component system regulates stress responses, drug sensitivity, sexual development, and virulence of *Cryptococcus neoformans*. *Mol. Biol. Cell***17**, 3122–3135 (2006).
17. Nakayama, Y., Hirata, A. & Iida, H. Mechanosensitive channels Msy1 and Msy2 are required for maintaining organelle integrity upon hypoosmotic shock in *Schizosaccharomyces pombe*. *FEMS Yeast Res*. **14**, 992–994 (2014).
18. 18. Chen, L. Y. et al. The *Arabidopsis* alkaline ceramidase TOD1 is a key turgor pressure regulator in plant cells. *Nat. Commun*. **6**, 6030 (2015)
19. Thines, E., Weber, R. W. S. & Talbot, N. J. MAP kinase and protein kinase A-dependent mobilization of triacylglycerol and glycogen during appressorium turgor generation by *Magnaporthe grisea*. *Plant Cell* **12**, 1703–1718 (2000)
20. Penn, T. J. et al. Protein kinase C is essential for viability of the rice blast fungus *Magnaporthe oryzae*. *Mol. Microbiol*. **98**, 403–419 (2015).
21. Raad, H. et al. Regulation of the phagocyte NADPH oxidase activity: phosphorylation of gp91^{phox}/NOX2 by protein kinase C enhances its

diaphorase activity and binding to Rac2, p67^{phox}, and p47^{phox}. *FASEB J*. **23**, 1011–1022 (2009).
22. Mithoe, S. C. et al. Attenuation of pattern recognition receptor signaling is mediated by a MAP kinase kinase kinase. *EMBO Rep*. **17**, 441–454 (2016).
23. Yin, Z. et al. Phosphodiesterase MoPdeH targets MoMck1 of the conserved mitogen-activated protein (MAP) kinase signalling pathway to regulate cell wall integrity in rice blast fungus *Magnaporthe oryzae*. *Mol. Plant Pathol*. **17**, 654–668 (2016).
24. Osés-Ruiz, M., Sakulkoo, W., Littlejohn, G. R., Martin-Urdiroz, M. & Talbot, N. J. Two independent S-phase checkpoints regulate appressorium-mediated plant infection by the rice blast fungus *Magnaporthe oryzae*. *Proc. Natl Acad. Sci. USA* **114**, E237–E244 (2017).
25. Gupta, Y. K. et al. Septin-dependent assembly of the exocyst is essential for plant infection by *Magnaporthe oryzae*. *Plant Cell* **27**, 3277–3289 (2015).
26. Soanes, D. M., Chakrabarti, A., Paszkiewicz, K. H., Dawe, A. L. & Talbot, N. J. Genome-wide transcriptional profiling of appressorium development by the rice blast fungus *Magnaporthe oryzae*. *PLoS Pathog*. **8**, e1002514 (2012).
27. Talbot, N. J., Salch, Y. P., Ma, M. & Hamer, J. E. Karyotypic variation within clonal lineages of the rice blast fungus, *Magnaporthe grisea*. *Appl. Environ. Microbiol*. **59**, 585–593 (1993).
28. Sambrook, J., Fritsch, E. F. & Maniatis, T. *Molecular Cloning: a Laboratory Manual* 2nd edn (Cold Spring Harbor Laboratory Press, New York, 1989).
29. Hamer, J. E. et al. A mechanism for surface attachment in spores of a plant pathogenic fungus. *Science* **239**, 288–290 (1988).
30. Kankanala, P., Czymmek, K. & Valent, B. Roles for rice membrane dynamics and plasmodesmata during biotrophic invasion by the blast fungus. *Plant Cell* **19**,
31. Mentlak, T. A. et al. Effector-mediated suppression of chitin-triggered immunity by *Magnaporthe oryzae* is necessary for rice blast disease. *Plant Cell* **24**, 322–335 (2012).
32. Lindsay, R. J., Kershaw, M. J., Pawlowska, B. J., Talbot, N. J. & Gudelj, I. Harbouring public good mutants within a pathogen population can increase both fitness and virulence. *eLife* **5**, e18678 (2016).
33. Kershaw, M. J. & Talbot, N. J. Genome-wide functional analysis reveals that infection-associated fungal autophagy is necessary for rice blast disease. *Proc. Natl Acad. Sci. USA* **106**, 15967–15972 (2009).
34. Petre, B., Win, J., Menke, F. L. H. & Kamoun, S. Protein–protein interaction assays with effector–GFP fusions in *Nicotiana benthamiana*. *Methods Mol. Biol*. **1659**, 85–98 (2017).
35. Bender, K. W. et al. Autophosphorylation-based calcium (Ca^{2+}) sensitivity priming and Ca^{2+}/calmodulin inhibition of *Arabidopsis thaliana* Ca^{2+}-dependent protein kinase 28 (CPK28).*J. Biol. Chem*. **292**, 3988–4002 (2017).
36. Anders, S. & Huber, W. Differential expression analysis for sequence count data. *Genome Biol*. **11**, R106 (2010).
37. Trapnell, C. et al. Transcript assembly and quantification by RNA-seq reveals unannotated transcripts and isoform switching during cell differentiation. *Nat. Biotechnol*. **28**, 511–515 (2010).
38. Soanes, D. M., Chakrabarti, A., Paszkiewicz, K. H., Dawe, A. L. & Talbot, N. J. Genome-wide transcriptional profiling of appressorium development by the rice blast fungus *Magnaporthe oryzae*. *PloS Pathog*. **8**, e1002514 (2012).

39. Ludwig, C., Claassen, M., Schmidt, A. & Aebersold, R. Estimation of absolute protein quantities of unlabeled samples by selected reaction monitoring mass spectrometry. *Mol. Cell. Proteomics* **11**, M111.013987 (2012). 40. Chojnacki, S., Cowley, A., Lee, J., Foix, A. & Lopez, R. Programmatic access to bioinformatics tools from EMBL–EBI update: 2017. *Nucleic Acids Res*. **45**, W550–W553 (2017).
40. Chojnacki, S., Cowley, A., Lee, J., Foix, A. & Lopez, R. Programmatic access to bioinformatics tools from EMBL–EBI update: 2017. *Nucleic Acids Res*. **45**, W550–W553 (2017).

Acknowledgements

We acknowledge technical support from O. Goode and T. Penn. This work was funded by a European Research Council (ERC) Advanced Investigator Award to N.J.T. under the European Union's Seventh Framework Programme (FP7/2007-2013), ERC grant no. 294702 GENBLAST. L.S.R. acknowledges the late P. Ryder for support and encouragement.